HAL
open science

Simulation of Single Particle Displacement Damage in Silicon – Part II: Generation and Long-Time Relaxation of Damage Structure

Antoine Jay, Melanie Raine, Nicolas Richard, Normand Mousseau, Vincent Goiffon, Anne Hémeryck, Pierre Magnan

To cite this version:

Antoine Jay, Melanie Raine, Nicolas Richard, Normand Mousseau, Vincent Goiffon, et al.. Simulation of Single Particle Displacement Damage in Silicon – Part II: Generation and Long-Time Relaxation of Damage Structure. IEEE Transactions on Nuclear Science, 2017, 64 (1), pp.141-148. 10.1109/TNS.2016.2628089 . hal-01407740

HAL Id: hal-01407740

https://hal.science/hal-01407740

Submitted on 2 Dec 2016

HAL is a multi-disciplinary open access archive for the deposit and dissemination of scientific research documents, whether they are published or not. The documents may come from teaching and research institutions in France or abroad, or from public or private research centers.

L'archive ouverte pluridisciplinaire **HAL**, est destinée au dépôt et à la diffusion de documents scientifiques de niveau recherche, publiés ou non, émanant des établissements d'enseignement et de recherche français ou étrangers, des laboratoires publics ou privés.

Simulation of Single Particle Displacement Damage in Silicon – Part II: Generation and Long-Time Relaxation of Damage Structure

Antoine Jay, *Member IEEE*, Mélanie Raine, *Member IEEE*, Nicolas Richard, *Member IEEE*, Normand Mousseau, Vincent Goiffon, *Member IEEE*, Anne Hémeryck, Pierre Magnan, *Member, IEEE*

Abstract **–A statistical study of displacement cascades induced by silicon Primary Knock-on Atoms (PKA) in bulk silicon is performed by running a large number of molecular dynamics (MD) simulations. The choice of the PKA species and energy varying from 1 to 100 keV comes from a previous particle-matter simulation [1]. The electronic stopping power missing in standard MD simulations is here taken into account using the Two Temperature Model (TTM). This prevents from overestimating the number of created defects. The damaged atomic structures obtained after one nanosecond of MD simulation are not representative of what is observed in image sensors for example after several minutes. For this reason, the kinetic Activation Relaxation Technique (k-ART) is used in a second step, allowing to access longer simulation times of up to second. The obtained damaged structures can then be compared with experimental observations. Analysis reveals two possible links between the simulated structures and the measurements in solid-state image sensors. First, the cluster size distribution exhibits a shape similar to the measured exponential distribution of Dark Current (DC). Second, the temporal evolution of metastable atomic configurations resembles experimental DC-Random-Telegraph-Signals.**

Index terms**– Silicon, Displacement Damage, Molecular Dynamics, kinetic Activation Relaxation Technique, Defects, Dark current, Random Telegraph signal.**

I. INTRODUCTION

While displacement damage (DD) effects have been studied for a long time on various types of devices (diodes, bipolar transistors, image sensors...), a fundamental understanding of the link between the changes at the atomic structure level and the resulting electrical effect measured on devices remains to be achieved [2]. One of the key barriers limiting this understanding is the difficulty to replicate numerically the evolution of damaged structures on realistic observable timescales compatible with available experimental data. Indeed, molecular dynamical (MD) approaches often used to generate damage structures at the atomic level only treat timescales up to nanoseconds. This is far from the timescale of experimental data generally spanning from milliseconds to days. Simulations using such *ab initio* molecular dynamics have also been performed previously (see for example [3,4]) but this kind of simulation is too limited in time and size to describe realistic displacement cascades.

To solve this issue, a comprehensive simulation project is developed, combining different techniques, in order to simulate the succession of phenomena, from the interaction between the incident particle and the target material, to the resulting electrical effect measured at the device level. This approach is described in details in a dedicated paper corresponding to the first part of this study [1], and summarized in the schematic of Fig.1. Because of the complexity of this project and because each step can lead to its own interesting conclusions, we choose to dedicate one paper to each simulation step. The first step simulating the incident particle interaction with the target material using Monte Carlo (MC) methods is described in [1]. This paper is devoted to the second step, corresponding to the generation of damage by a Primary Knock-On Atom (PKA) in the crystalline structure and the temporal evolution of the resulting defect structure. To achieve this, two different simulation tools are used.

First, MD simulations are performed to generate the damage structure and to observe its evolution up to nanoseconds. The novelty in this paper lies in the simulation of rather large PKA energies, compared to previous papers (see for example [5]), corresponding to realistic cases generated by the primary interaction and determined in the MC step in [1]. Moreover, special care is given to the consideration of electronic stopping power in the MD simulations, using the Two-Temperature Model (TTM) introduced by Duffy *et al.* [6]. Finally, these simulations are performed on a large number of PKA directions in order to be as realistic as possible and to construct a statistically significant database of damaged structures.

The second step detailed in this paper uses a new algorithm called the kinetic Activation Relaxation Technique (*k-ART*) [7]. This technique allows the evolution of the damage structure at a fixed temperature on much longer timescales than usual studies, *i.e.* up to seconds and more after the damage generation. This approach thus avoids the use of thermally activated annealing, which can generate misleading reaction barriers and structures because of the artificially accelerated

A. Jay, V. Goiffon and Pierre Magnan are with ISAE, Université de Toulouse, 10 av. E. Belin, F-31055 Toulouse, France (antoine.jay@isae.fr).
M. Raine, and N. Richard are with CEA, DAM, DIF, F-91297 Arpajon, France (melanie.raine@cea.fr).
N. Mousseau iswith Université de Montréal, C.P. 6128, Succursale Centre-Ville, Montréal, CA-H3C 3J7, Québec, Canada (normand.mousseau@umontreal.ca).
A. Hémeryck is with LAAS/CNRS, 7, av. du Col. Roche, F-31031 Toulouse, France (anne.hemeryck@laas.fr).

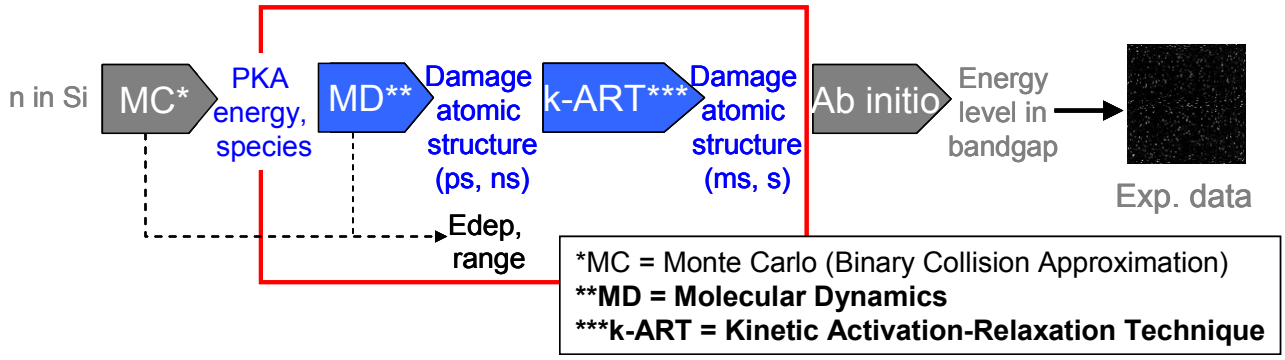

Fig.1 : Schematic of the global simulation project. The steps inside the scope of this paper are identified by red squares.

structural relaxation. Here the *k-ART* algorithm has been used at 300 K, which is the temperature at the end of the MD step.

The final goal of this paper is to identify complex defect structures still present in the material after seconds and that could be associated with experimental measurements of Dark Current (DC) or Dark Current Random Telegraph Signal (DC-RTS) in solid-state image sensors [8].

The paper is organized as follows: in Sec. II, the two simulation steps and their computational details are described. In Sec. III, the MD-TTM results are given, the cascade properties and the generated defects are analyzed and discussed through a comparison with results coming from *SRIM* [9] and *Geant4* [10,11] codes. Then, Sec. IV is devoted to the results obtained from the *k-ART* calculations. Results of the damage structure evolution after seconds are then analyzed, allowing the identification of different configurations of stable defects. Moreover, the analysis also reveals the presence of "flickering" defects, *i.e.* damage structures which switch between a limited number of configurations over time. These "flickers" are discussed in relation with the Dark Current phenomena measured in image sensors. Finally, Sec. V summarized the main conclusions and gives perspectives regarding the next step of our approach.

II. Methodology

A. Molecular Dynamics

MD simulations are performed with the *LAMMPS* code [12] to access the atomic scale of defect configurations generated by the PKA. The simulation supercell contains 1 million silicon atoms in their diamond-like crystalline form. They interact together via the Stillinger-Weber (SW) potential [13]. The simulated system evolves during 1 ns, with an increasing time step varying from 0.001 to 10 fs as the velocity of the atoms decreases. The structure does not evolve anymore during the last steps.

The Two-Temperature Model (TTM) [6,14] is used in order to take into account the electronic stopping power in addition to the force field governing the shocks between the atoms. This model provides a mechanism for energy exchange between radiation-excited carrier gas and atoms. When TTM is not used, as it is the case by default in standard MD, this leads to too high penetration ranges. This overestimation depends on the studied material and is approximately of 150% in bulk silicon. Indeed, if not included, all the kinetic energy of incident particles is lost through non-ionizing interactions, thus also overestimating the resulting damage. This TTM model has been mainly used for metals [6,15] or insulators [16,17]. It has also been used for semiconductors [18,19] but, to our knowledge, never with temperature dependent parameters. The temperature dependency has been estimated through the electronic specific heat C_e in eV/(e^-.K) as follow:

$$C_e(X) = 1.29.10^{-4} + (-1.2899.10^{-4} - 2.93276.10^{-8}X + 2.29991.10^{-5}X^2 + 9.27036.10^{-7}X^3)e^{-(0.42485409X)^2}$$

with $X=T_e/1000$ where T_e is the electronic temperature. C_e is obtained from a fit of experimental data [20] at low temperature and of a free electron gas ($3/2*k_b*T$) above the Fermi temperature $T_F = E_F/k_b = 0.56$ eV/k_b =6 498 K where k_b is the Boltzmann constant.

The other parameters independent from temperature involved in the TTM model are:

- The electronic density is taken as ρ_e=0.05 e^-/Å^3 assuming that each atom can give one electron for the electronic thermal transport [21].
- The electronic thermal diffusivity: D_e=20 000 Å^2/ps [21] is the one of molten metal as the electronic temperatures obtained in the simulations are really high.
- The electron-phonon friction coefficient γ_p=1.741 g/(mol.ps) is the one optimized by Chettah *et al.* [22] for TTM simulations.
- The electron stopping power coefficient: γ_s=39.23 g/(mol.ps) is obtained with SRIM tables in the Lindhard and Sharff model [23] using silicon PKA in bulk silicon.
- The electronic stopping critical velocity v_0=79.76Å/fs is taken as being two times the cohesive energy 4.63 eV [24].
- The grid of finite volume on which the equations of diffusion are solved in the electronic subsystem is 20*20*20.

At the beginning of the simulation, all the atoms have a random velocity corresponding to a temperature of 300 K. Then, to start the simulation, one atom, the PKA, is given an initial velocity corresponding to the wanted kinetic energy. The chosen energies (1 and 10 keV) and species (silicon atoms) come directly from a selection of relevant

PKA in the outputs of the Monte Carlo (MC) calculations performed in [1]. The use of this very large PKA energy for MD allows the simulation of realistic cases, representative of the kind of damages generated by incident neutrons or protons from hundreds of keV to hundreds of MeV. As detailed in the following, 10 keV PKA indeed leads to the creation of clusters of defects that are large enough to form amorphous pockets larger than 20 unit cells and that do not re-crystallize totally during the annealing step. Some 100 keV simulations are also performed to validate the choice of these representative energies, checking that larger incident PKA energies do not induce larger clusters.

A large number of simulations is performed (100) for each incident energy. Each of them can be distinguished by its PKA initial direction. The set of all these directions is equally distributed all over the space to optimize the sampling of the possible directions that can result from the particle-matter interaction. This permits to access good statistics on the resulting damaged structures.

Indeed, the penetration depth and the number of defects vary drastically with the PKA direction. As it is then impossible to draw conclusions from only one simulation, a statistic study based on numerous simulations is then mandatory. As an illustration, the penetration depths of the 100 simulations performed for a 10 keV PKA with different incident directions are given in Fig. 2. This histogram shows that each of the 100 incident directions produces a different penetration depth. For this reason, it is inaccurate to deduce the cascade properties from only one simulation. Furthermore, the standard deviation of this histogram increases with the PKA energy, justifying even more the need of statistical results for this kind of study.

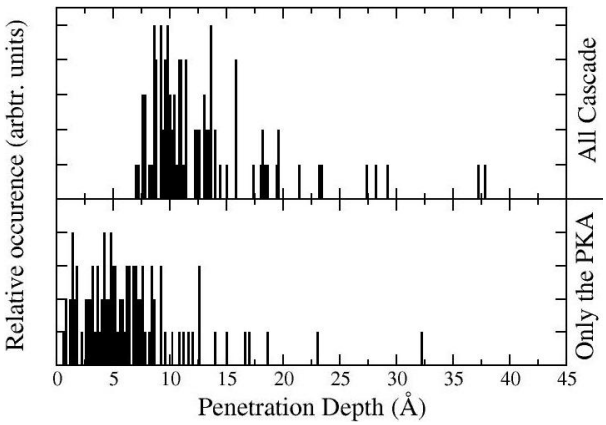

Fig. 2: Distribution of the penetration depths of the cascade (above) and of the PKA (below) for the 100 different incident directions for 10 keV PKA.

Hence, this MD-TTM approach has three main improvements: the use of TTM, of realistic PKA energies and of statistics on different incident directions. The result of this simulation step is a collection of 100 damaged atomic structures. Since this step only simulates the first nanosecond of the life of the structures, it is not relevant to directly compare them to the experimental observations that occur several minutes after the irradiation. The long time scale annealing needed to do this comparison can be done using the Activation Relaxation Technique in its kinetic format (*k-ART*).

B. k-ART

The kinetic Activation Relaxation Technique (*k-ART*) [7] is a self-learning and off-lattice kinetic Monte Carlo algorithm based on the Activation-Relaxation Technique nouveau (*ARTn*) [25]. This method allows the exact treatment of elastic effects both for energy minima and saddle points in complex materials in order to follow the time evolution of large simulation boxes over timescales up to seconds or more. The principle is to go out of the potential well of the ongoing atomic configuration by searching an energetically more favorable one. The method is separated in two steps.

The first one consists in the exploration of all the atomic configurations of the energy landscape separated by only one maximum (*i.e.*, the nearest valleys). An event is then defined through three atomic configurations: the starting one, the final one and the saddle point. The transition probability is calculated from their potential energy differences. Events are then classified based on the local topology which allows the study of disordered environments without any reference to a crystalline reference lattice. At each steps, all low energy barriers, associated with a probability of at least 0.01 per cent, are then reconstructed and fully relaxed to account for elastic deformation induced by the structural evolutions.

The second step follows the standard kinetic Monte Carlo algorithm, which computes the time step based on the rates of events for the specific structure and selects one move from the initial configuration to another. The catalog of possible configurations is then updated if necessary and the event lists reconstructed to account for the change in topology before applying the kinetic MC step again.

With its efficiency flicker handling algorithm and its use of local-force calculations, this algorithm has already proved its efficiency on the simulation of a number of complex materials including metallic alloys and relaxation of ion-implanted silicon with system sizes ranging from a few hundred to many tens of thousands of atoms [7]. Similarly to the MD-TTM simulations, the result of these simulations is also a library of damaged atomic structures, but relaxed on timescales more similar to the experimental ones. Due to computational cost, only some of the 100 MD-TTM final configurations are annealed with the *k-ART* code (between 1 and 10 depending on the energies), chosen amongst the most common ones.

III. MD-TTM SIMULATIONS RESULTS

A. Steps of the cascade

As illustrated in Fig. 3, five main steps can be distinguished in the formation of the cascade. First (Fig. **3**a), the PKA (in red in the figure) shocks the Secondary Knock-on Atoms (SKA, in blue) with high velocity. SKA are far from each other: on average 4 nm for a 10 keV PKA. Second (Fig. 3b), the SKA transmit their energy to the surrounding atoms still with a high velocity. These two steps correspond to the ballistic propagation and determine the width and depth of the cascade. Third (Fig. 3c), those atoms give their energy to create interstitial atoms and vacancies. They form amorphous pockets when close enough. Fourth (Fig. 3d), the elastic thermal wave

propagates and moves the atoms with a displacement so small that they come back to their initial crystalline positions (this corresponds to transmitted energies lower than the 21 eV required to displace an atom in silicon). Fifth (Fig. 3e), with the residual energy, a large part of the isolated Frenkel pairs (~50%) recombine to reform the crystal.

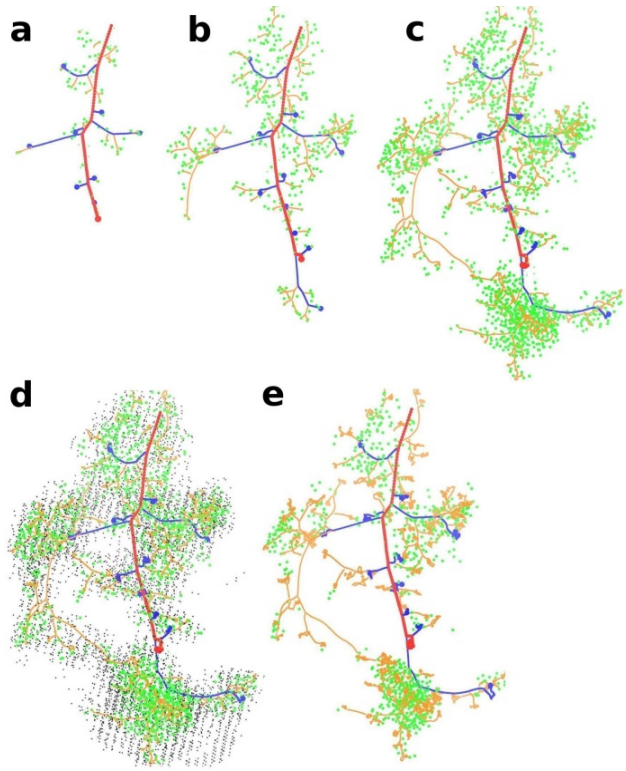

Fig. 3: The five characteristic steps occurring during the MD-TTM propagation of the cascade of defects. Red balls: positions of the PKA. Blue balls: positions of the SKA. Orange balls: positions of the atoms shocked with a high velocity but not by the PKA. Green balls: positions of the atoms with low velocities. Black balls: positions of the atoms involved in the thermal wave (movie available as supplementary material).

B. Characterization of the defects along the cascade

Two main groups of defects are observed along the cascades: the point defects and the extended defects.

Regarding point defects, *i.e.* isolated vacancies and interstitial atoms, the remaining vacancies (V) at the end of the simulation generally correspond to the original positions of the PKA and the SKA that move far away from their initial crystalline site. They are then located at the beginning of the cascade. On the contrary, the PKA and SKA become interstitial atoms (I) that are mainly located at the extremity of the cascade, *i.e.* in the amorphous pockets. For this reason, those pockets or clusters have generally an excess of atoms, whereas simple isolated defects are generally atom deficient (*i.e.* related to vacancies). An example of final structure is given in Fig. 4.

Those clusters form extended defects whose sizes and shapes vary. In the following, we define the size of a cluster as the longest edge of the smallest rectangular parallelepiped that contains the entire cluster and we consider that two defects are in the same cluster if the distance between them is lower than two times the crystalline interatomic distance, *i.e.* 2x2.35=4.7 Å in silicon. This allows distinguishing three kinds of clusters: the small ones, the medium ones and the large ones. Each of them will have its own behavior during the annealing step. Small clusters are the only ones simple enough to be easily categorized: they are formed by a bi, a tri or a quadri-vacancy (2V, 3V, 4V), or by a bi a tri or a quadri-interstitial atom (2I, 3I, 4I). Some of them are presented in Fig. 11 and discussed in [26]. The medium clusters involve from tens to hundreds of defects; they are not dense enough to be called amorphous pockets. The large clusters are formed by more than one thousand defects and seem very similar to amorphous silicon.

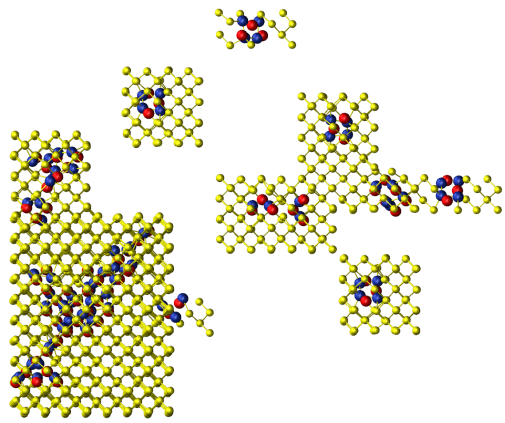

Fig. 4: Examples of clusters generated by a 1 keV PKA. Blue balls represent interstitial atoms, red balls vacancies and yellow balls silicon atoms that remain on a regular crystalline site.

Depending on the PKA energy, general trends can be drawn from this first MD step.

For 1 keV PKA simulations, the final configurations are generally composed of two to ten isolated point defects and small clusters, and of one or two medium clusters involving 30 to 200 defects. An example of these final configurations is given in Fig 4.

For 10 keV PKA simulations, the final configurations are generally composed of ten to fifty point defects and small clusters, 3 to 10 medium clusters, and one or two large clusters.

For 100 keV PKA simulations, the results are relatively similar to 10 keV PKA simulations, except that the number of clusters of each type is larger. The fact that the large clusters have nearly equivalent sizes compared to those generated by 10 keV PKA simulations is not surprising. In fact, in these large energy simulations, the mean free path of the SKA is larger than the largest size of the amorphous pockets generated by 10 keV PKA. For this reason, the clusters of two SKA with an energy superior to 10 keV cannot overlap to form a larger cluster. Hence, 10 keV seems to be a good compromise, leading to amorphous pockets which sizes are also representative of the ones created by incident PKA with energies larger than 10 keV. This validates the choice made from analysis of neutron-silicon MC simulations in [1].

The cluster size distribution at the end of MD simulations is given in Fig. 5 for 100 simulations of 10 keV PKA. It has an exponential shape that resembles the exponential shape of the dark current (DC) distribution measured in CMOS image sensors [27]. While the size of clusters is expected to decrease in the following *k-ART*

simulation step, the shape of the curve should remain similar, only shifted to smaller cluster sizes. This resemblance could be evidence of the instinctive assumption that a small DC value is due to the presence of small clusters in the silicon photo-diode, whereas a large DC value is due to the presence of large amorphous areas in the irradiated photo-diode. This assumption still needs to be proven, for example by the calculation of the electronic quantum states in the clusters band gap. This is the last part of our global simulation project presented in Fig. 1, involving *ab-initio* calculations, and will be the subject of future papers.

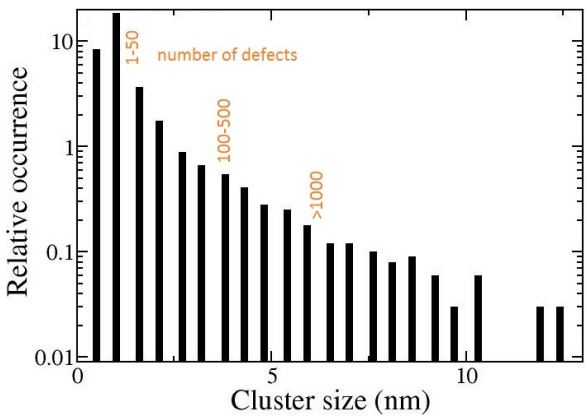

Fig. 5: Distribution of the size of the clusters generated by 10 keV PKA. Histogram coming from the last step of the 100 MD-TTM simulations at 1 ns. Orange numbers give the average number of defects per cluster.

C. Cascade properties – comparison with Geant4 results

The histogram of the number of secondary knocked-on atoms (SKA) generated by a 10 keV PKA is given in Fig. 6. It is compared to the results obtained with *Geant4* (for details on the *Geant4* calculations, see [1]). The average value obtained with MD-TTM is slightly lower than the one obtained with *Geant4*, but the order of magnitude is the same. In fact, the Binary Collision Approximation used in *Geant4* is only considered valid beyond 1 keV. On the contrary, 100 keV is the upper value that limits the domain in which MD simulations are feasible due to the exponential increase of computational time. Hence, the comparison can only be done in a small range of value (1 to 100 keV), and the difference between the two models decreases with increasing the PKA energy increases.

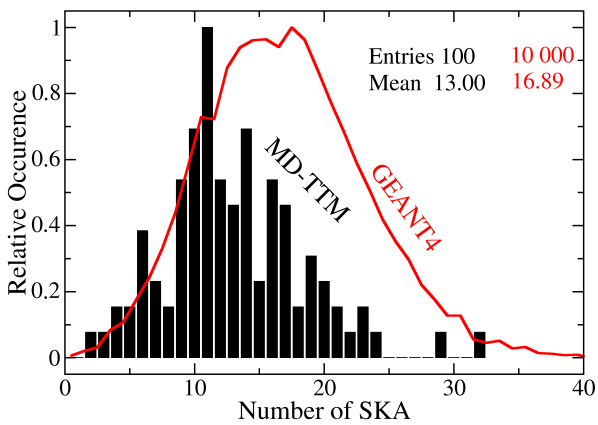

Fig. 6: Distribution of the number of SKA in a 10 keV PKA cascade formed by MD-TTM (in black) and by the binary collision approximation (*Geant4* in red).

D. Limits of Molecular Dynamics

The evolution of the number of defects as a function of time is given in Fig. 7. It is compared to a value coming from the *SRIM* code in full cascade mode, often used as reference for this kind of calculation. It shows that, even with the addition of the TTM, the number of defects obtained at the end of the MD-TTM run (1 ns) is larger than the *SRIM* value. In Fig. 7, we represent the time evolution up to 100 ps, because the number of defect doesn't change between 100 ps and 1 ns in MD. This difference comes not only from the shortness of the time scale accessible with the MD technique, but also from the fact that this simulation method makes impossible the access to other configurations. The use of the *k-ART* algorithm is a way to address this issue, as detailed in the next section.

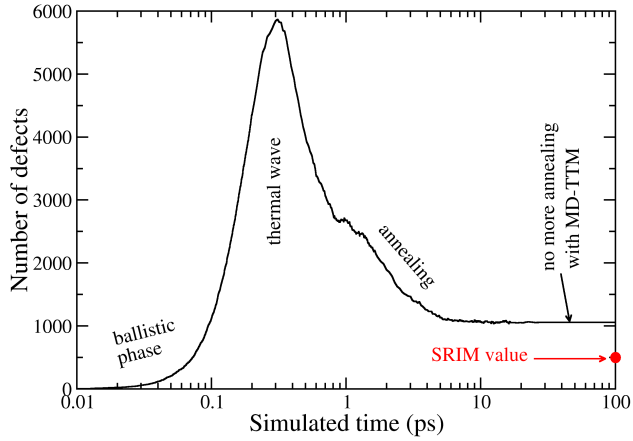

Fig. 7: Temporal evolution of the number of defects during MD-TTM for an initial PKA of 10 keV. The red point corresponds to the final number of vacancies given by *SRIM*. As the simulation begins with a perfect cristal, the number of interstitial atoms and of vacancies is the same and is here named number of defects.

IV. *k-ART* Results

In this section, starting from atomic configurations obtained at the end of the MD simulation, we first describe the global annealing behavior of the damaged structure on long timescale accessible with *k-ART*. The annealing behavior of defects is then analyzed depending on their size. Finally we underline the particular defect structures that could be linked to DC and DC-RTS.

A. Global behavior

The evolution of damaged structure can be roughly split in four main parts, each of them having its own time scale.

First, unstable atomic configurations are stabilized very rapidly (~1 ns) locally during the first microseconds of the simulation. Indeed, the energy barriers that need to be overcome for their annealing do not exceed 0.2 eV. These configurations are part of the medium and large clusters.

Second, Frenkel pairs anneal also very rapidly (in ~100 ns).

Third, mono-vacancies (V), mono-interstitials (I) and bi-interstitial (2I) diffuse, because of their low energy barriers until they join into an amorphous pocket or meet another defect either to form a small cluster or to recrystallize.

Fourth, after ~1 s, only small clusters and residual large

clusters are still present around the cascade and main evolutions occur over longer timescales (one event per minute or longer). This is due to the fact that the system reaches a single potential well surrounded by high energy barriers (> 0.8 eV), corresponding to a meta-stable configuration. These long-changing events involve the global displacement of a large number of atoms that is typically larger than 15.

All these processes lead to a drastic diminution of the number of defects present in the structure, as shown in Fig. **8**. This number is then in good agreement with the *SRIM* value, which was not the case after MD-TTM simulations. Examples of configurations reached after several seconds of simulation are presented in Fig. 11.

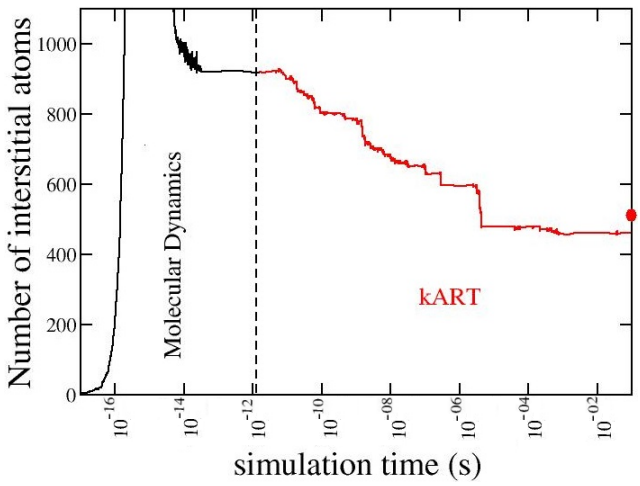

Fig. 8: Temporal evolution of the number of interstitial atoms (= number of vacancies) during MD-TTM (black curve) for an initial PKA of 10 keV (same curve as in Fig. 7) and during *k-ART* annealing (red curve). The red dot indicates the value given by the *SRIM* code.

Fig. 9 represents an example of the occurrence of each type of clusters at the end of the *k-ART* simulation (here after 1 minute) compared to the end of MD simulation (1 ns), for one direction of 1 and 10 keV PKA.

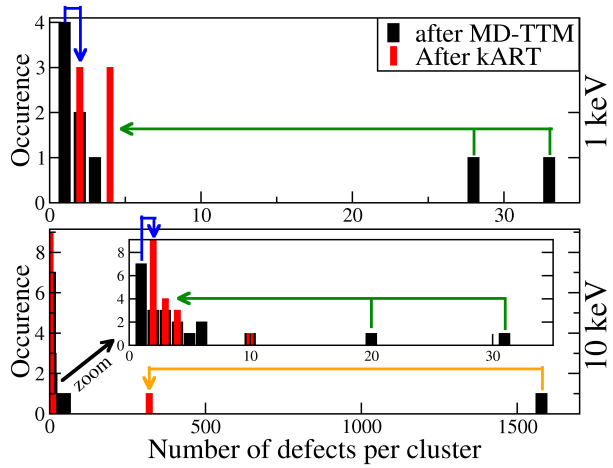

Fig. 9: Examples of the variation of the number of defects per clusters for a 1 keV PKA simulation (top) and for a 10 keV PKA simulation (bottom).Black histogram: last step of MD-TTM simulation (1 ns). Red histogram: last step of *k-ART* simulation (1 min). Blue arrows: agglomeration of point defects. Green arrows: medium clusters total annealing. Orange arrow: large cluster partial annealing.

B. Behavior of point defects and small clusters

The three most simple defects, the mono-vacancy (V), the mono-interstitial (I) and the bi-interstitial (2I) have a different behavior than other small clusters. Those three defects are the only ones to diffuse rapidly in the crystal structure, because of their low diffusion energy barriers. Indeed, we find energy barriers of 0.51, 0.78 and 0.28 eV for V, I and 2I respectively compared to 1.00, 1.32, 1.52, 1.66 and 1.10 eV for 2V, 3V, 4V, 3I and 4I respectively. These values are in perfect agreement with [26]. However, their migration is not random if other defects are close enough to them, so that they feel the lattice distortion induced by those surrounding defects. This distortion leads to an agglomeration of the defects. This is due to the potential energy of the so created cluster that is lower than the sum of the potential energies of the separated defects. If the agglomerated cluster is composed of an interstitial atom and a vacancy, *i.e.* a Frenkel pair, it re-crystallizes in a few microseconds. Otherwise, it forms a small cluster (2V, 3V, 4V, 3I or 4I) that does not diffuse anymore.

For this reason, all of these 3 simple defects formed during the cascade are not present at the end of the annealing (> 1 s). This behavior is described by the blue arrows in Fig. 9. On the contrary, the number of small clusters increases during annealing since simple defects agglomerate. This number cannot actually decrease because the migration energy barrier of small clusters is too high to allow their diffusion. Moreover, their V or I overage make their whole re-crystallization impossible. As shown in Fig. 9, this behavior is the same for all defects structures whatever the energy of their original PKA (1 keV or 10 keV).

C. Behavior of medium versus large clusters

The larger the PKA energy, the larger the size of the amorphous pockets or clusters located at the extremity of the cascade obtained by MD. There is a limit, located between 1 and 10 keV, which separates two kinds of phenomenon.

First, when these clusters generated by MD are small enough (medium clusters), *i.e.* typically composed of less than 200 non-crystalline atoms, they can totally re-crystallize with time. This annealing is indicated by the green arrows in Fig. 9. If the number of vacancies (nV) and of interstitial atoms (nI) in one cluster is not the same, this total re-crystallization is not possible. In this case, the cluster quasi-re-crystallizes with time, leading to a small cluster, typically formed by a bi, a tri, or a quadri-interstitial atom or vacancy as a function of the difference nV-nI. As this number rarely exceeds 3 or 4, small clusters larger than 4V or 4I are very unusual. Nevertheless, they are sometimes formed by the agglomeration of a resulting 4V or 4I and of a diffusing point defect.

Second, when the clusters generated at the end of MD are large enough (large clusters), typically when they are composed of more than 1000 non-crystalline atoms, their annealing takes a longer time and is rarely total. This annealing is indicated by the orange arrow in Fig. 9. This difference of behavior between medium and large clusters is due to the fact that the re-crystallization of large amorphous pockets occurs simultaneously at different places. This leads to a non-uniform repartition of V and I forbidding their total annealing. Thus, a large cluster becomes an agglomeration of many closely spaced small clusters that are hardly distinguishable by experimentalists

as their separating distance is lower than 4.7 Å. For this reason, what we name an "agglomeration of small clusters" that we are able to differentiate after annealing, is commonly named an amorphous pocket by experimentalists. Despite this, the size of the large clusters drastically decreases during annealing. They become smaller and more stable amorphous pockets than after MD-TTM. In the 10 keV PKA cascade annealing given as an example in Fig. 9, the large cluster is formed by 1500 defects at the last step of MD (1 ns) and by only 300 defects at the last step of the *k-AR*T algorithm (1 min).

D. Flickering structures

In most cases, a final configuration continues to evolve even after days of annealing. However, this evolution is not a total defect annealing, but a cyclic switch between a finite number of configurations. In fact, the final system is trapped into several potential wells, separated by small energy barriers. This wells form a basin that is surrounded by insurmountable high energy barriers as shown in Fig. **10**a). As the system can thermally switch between all the configurations into the basin, we name this switching topology a "flicker". An average lifetime can be attributed to each of its atomic configurations as a function of the calculated energy barriers. It is then possible to evaluate their evolution as a function of time as shown in Fig. 10b). These evolutions seem very similar to the ones of the DC-RTS observed in CMOS Active Pixel Image Sensors (CMOS-APS) [7,28].

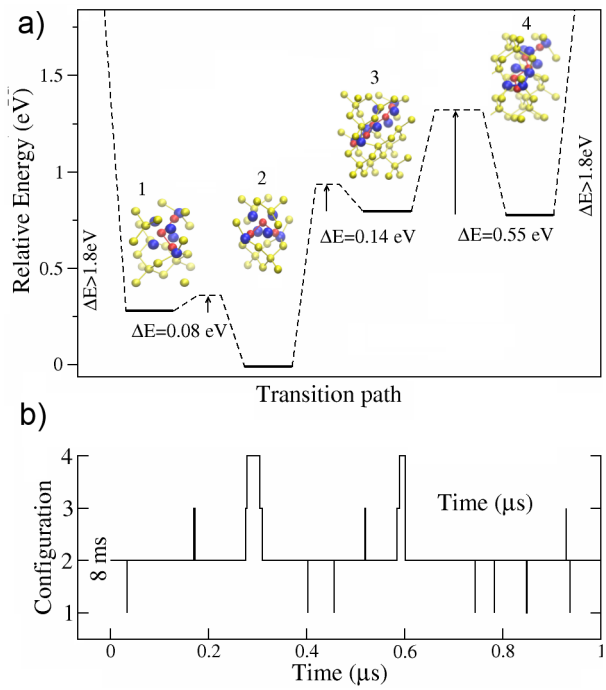

Fig. 10: An example of simple flickering configuration: the tri-interstitial. a): the four configurations, their relative energy and the energy barrier. b): time spend in each configuration after 8 ms of annealing.

The example of Fig. 10 is a small cluster: the 3I. The flicker switches between four configurations, two of them having tenth of microsecond lifetimes. This short lifetime is hardly observable experimentally. Thus this flicker is probably seen as a stable DC and not as a DC-RTS. This should be the same for all the small clusters. On the contrary, a cluster that still have hundreds of defects after annealing also forms a basin, containing more than thousands of metastable configurations. Among all of them, a dozen are surrounded by energy barrier superior to 0.8 eV, corresponding to an average lifetime of 10 s that is easily observable experimentally. This kind of structure could be the source of multi-levels DC-RTS.

E. Limits of k-ART

It is known from experimental data that transient annealing is very dependent on the excess carrier concentration present in bulk material or in a device [29].The annealing time can also be decreased due to an excess of charge-states that may modify the defects mobility [30].

To take these effects into account in the *k-ART* simulations and allow direct comparison with experimental data, nor our empirical potential (SW) neither those using a charge density (EAM) are adequate. In fact, the positions of the localized states in the gap, which result from a defect in the periodic crystalline structure, are directly affected by an excess or lack of charges. As a consequence, the defect's binding energies that govern its mobility are also modified. To evaluate them in a charged system, one then need to solve its Hamiltonian. This task requires *ab initio* calculations. This technique does not permit to treat sufficiently large systems due to the present computational cost. Dealing with interatomic potential is thus for the moment the best compromise that allows studying mesoscopic annealing including diffusion and displacement of a large number of atoms.

IV. CONCLUSION

To describe the displacement damage in silicon, we use an original approach coupling Molecular Dynamics and Two-Temperature Model followed by *k-ART*, using input data coming from the Monte Carlo particle-matter interaction code *Geant4*. The TTM allows to take into account the electronic stopping power in MD simulations. A large library of damage structures is then generated after 1 ns with MD-TTM. This large library of configurations is afterwards relaxed on long times with the *k-ART* algorithm, leading to a complete catalog of possible atomic moves with their appropriate attempt-frequencies and activation barriers. Different stable structures are identified, along with a possible source of DC-RTS, corresponding to the multi-levels flickers in amorphous pockets.

ACKNOWLEDGMENT

The authors would like to thank M. Trochet, M. Toutlemonde, J. Srour, P. Paillet, M. Gaillardin, L. Martin-Samos, S. Girard, JM. Belloir and C. Durnez for fruitful discussions. The computer simulations were performed using HPC resources from GENCI-CCRT (Grant 2016097474) and from CALMIP (Grant 1555).

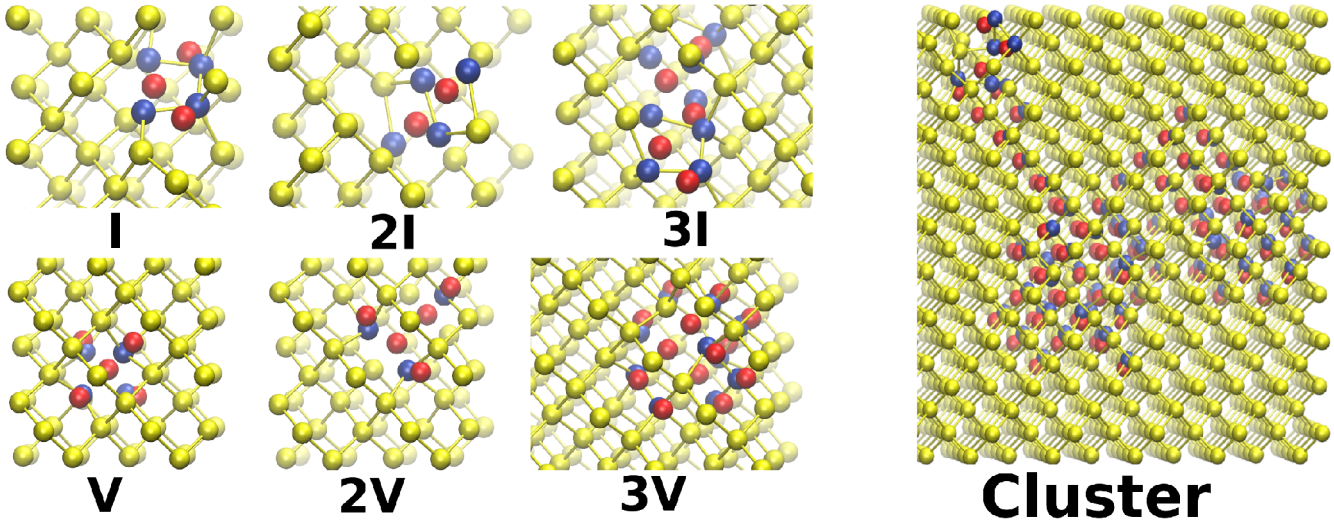

Fig. 11: Examples of point defects (I and V), of small clusters (2I, 2V, 3I, 3V) and of a large cluster obtained at the end of the annealing. All the clusters of defects have several possible configurations (flickers), and only the stable one are shown there.

REFERENCES

[1] M. Raine, N. Richard, A. Jay, V. Goiffon, S. Girard, M. Gaillardin and P. Paillet, "Simulation of single particle displacement damage in silicon – part I: global approach and primary interaction simulation", presented at NSREC2016 and submitted to *IEEE Trans. Nuc. Sci.*.

[2] J. R. Srour and J. W. Palko, "Displacement Damage Effects in Irradiated Semiconductor Devices", *IEEE Trans. Nuc.Sci*., vol. 60, pp. 1740, 2013.

[3] M. J. Beck, R. D. Schrimpf, D. M. Fleetwood, and S. T. Pantelides, "Disorder-recrystallization effects in low-energy beam-solid interactions," *Phys. Rev. Lett.*, vol. 100, pp. 185502, 2008.

[4] M. J. Beck, R. Hatcher, R. D. Schrimpf, D. M. Fleetwood, and S. T. Pantelides, "Quantum mechanical description of displacement damage formation," *IEEE Trans. Nucl. Sci.* 54, 1906-1912 (2007).

[5] G. Otto, G. Hoblera, and K. Gartner, "Defect characterization of low energy recoil events in silicon using classical molecular dynamics simulation," *Nucl. Instr .and Meth. B*, vol. 202, pp. 114–119, 2003.

[6] D. Duffy and A. Rutherford, "Including the effects of electronic stopping and electron-ion interactions in radiation damage simulations", *J. Phys.: Condens. Matter*, vol. 19, pp. 016207, 2007.

[7] L. K. Béland, P. Brommer, F. El-Mellouhi, J.-F. Joly and Normand Mousseau, "Kinetic activation-relaxation technique", *Phys. Rev. E*, vol. 84, pp. 046704, 2011.

[8] V. Goiffon, "Radiation Effects on CMOS Active Pixel UImage Sensors", in Ionizing Radiation Effects in Electronic: From Memories to Imagers, CRC Press, ch. 11, pp. 295-332, 2015.

[9] http://www.srim.org/

[10] S. Agostinelli, *et al*., "Geant4—a simulation toolkit", *Nucl. Instr. and Meth. A*, vol. 506, pp. 250-303, 2003.

[11] J. Allison, *et al*., "Geant4 Developments and Applications", *IEEE Trans. Nuc.Sci.,* vol. 53, pp. 270-278, 2006.

[12] S. Plimton, "Fast Parallel Algorithms for Short-Range Molecular Dynamics", *J.Comput. Phys*., vol. 117, pp. 1–19, 1995. Available on http://lammps.sandia.gov

[13] F. H. Stillinger and T. A. Weber "Computer simulation of local order in condensed phases of silicon", *Phys. Rev. B*, vol. 31, pp. 5262-5271, 1985.

[14] For documentation of the two-temperature model implemented in LAMMPS, see http://lammps.sandia.gov/doc/fix_ttm.html

[15] J. Chen, "A semi-classical two-temperature model for ultrafast laser heating," *International Journal of Heat and Mass Transfer*, vol. 49, pp.307–316, 2006.

[16] M. Toulemonde, J. Costantini, C. Dufour, A. Meftah, E. Paumier and F. Studer, "Track creation in SiO_2 and $BaFe_{12}O_{19}$ by swift heavy ions: a thermal spike description," *Nucl. Instr. and Meth. B*, vol. 116, pp. 37–42, 1996.

[17] M. Toulemonde, C. Dufour, A. Meftah, and E. Paumier, "Transient thermal processes in heavy ion irradiation of crystalline inorganic insulators," *Nucl. Instr . and Meth. B*, vol. 166-167, pp. 903–912, 2000

[18] J. Chen, D. Tzou, and J. Beraun, "Numerical investigation of ultrashort laser damage in semiconductors," *International Journal of Heat and Mass Transfer*, vol. 48, pp. 3–4, 2005.

[19] O. Osmani, I. Alzaher, T. Peters, B. d'Etat, A. Cassimi, H. Lebius, I. Monnet, N. Medvedev, B. Rethfled, and M. Scleberger, "Damage in crystalline silicon by swift heavy ion irradiation," *Nucl. Instr. and Meth. B*, vol. 282, pp. 43–47, 2012.

[20] C. Glassbrenner and G. Slack, "*Thermal conductivity of silicon and germanium from 3k to melting point*" Physical Review A, vol. 134, pp. 1058–1069, 1966.

[21] M. Toulemonde, C. Dufour, A. Meftah, and E. Paumier, "*Transient thermal processes in heavy ion irradiation of crystalline inorganic insulators*", Nuclear Instruments and Methods in Physics Research B, vol. 166-167, pp. 903–912, 2000.

[22] A. Chettah, H. Kucal, Z. Wang, M. Kac, A. Meftah, and M. Toulemonde, "*Behavior of crystalline silicon under huge electronic excitations: A transient thermal spike description*", Nucl. Instr. and Meth. in Phys. Res. B, vol. 267, pp. 2719–2724, 2009.

[23] J. Lindhard and M. Sharff, "Energy loss in matter by fast particles of low charge", Matematisk-fysiske Meddelelser det Kongelige Danske Videnskabernes Selskab, vol. 27, p. 15, 1953.

[24] B. Farid and R. Godby, "*Cohesive energies of crystals*", Physical Review B, vol. 43, p. 14248, 1991.

[25] R. Malek and N. Mousseau, "Dynamics of Lennard-Jones clusters: A characterization of the activation-relaxation technique", *Phys. Rev. E*, vol. 62, pp. 7723-7728, 2000.

[26] M. Trochet, L.K. Beland, J.F. Joly, P. Brommer and N. Mousseau,"Diffusion of point defects in crystalline silicon using the kinetic activation-relaxation technique method", *Phys. Rev. B*, vol. 91, pp. 224106, 2015.

[27] J.-M. Belloir, V. Goiffon, C. Virmontois, P. Paillet, M. Raine, P. Magnan, O. Gilard "Dark Current Spectroscopy in Proton, Carbon and Neutron Irradiated Pinned Photodiode

CMOS Image Sensors", presented at NSREC2016 and submitted to *IEEE Trans. Nuc. Sci.*.
[28] C. Durnez, V. Goiffon, C. Virmontois, P. Magnan, L. Rubaldo, "In-depth analysis on radiation induced multi-level dark current random telegraph signal in slicon solid state image sensors", *IEEE Trans. Nucl. Sci.,* vol. 64, 2017.
[29] J. Srour, C. J. Marshall, P. W. Marshall, "Review of displacement damage effects in silicon devices", *IEEE Trans. Nucl. Sci.,* vol. 50, pp. 653 – 670, 2003.
[30] B.L. Gregory, "Injection-stimulated vacancy reordering in p-type silicon at 76 K", *J. Appl. Phys.,* vol. 36, pp.3765-3769, 1965.